coatings

MDPI

Article

Characterization and Boron Diffusion Kinetics on the Surface-Hardened Layers of Royalloy Steel

Peter Orihel [1], Marián Drienovský [1], Zuzana Gabalcová [1], Peter Jurči [1,*] and Mourad Keddam [2]

[1] Faculty of Material Sciences and Technology of the STU in Trnava, J. Bottu 25, 917 24 Trnava, Slovakia
[2] Laboratoire de Technologie des Matériaux, Université des Sciences et de Technologie Houari Boumediène, Bab-Ezzouar 16111, Algeria
* Correspondence: p.jurci@seznam.cz

Abstract: The Royalloy steel was boronized at 1173, 1223, 1248, 1273 or 1323 K for 1, 3, 5, 7 or 10 h using a Durborid powder mixture. The boronized samples were analyzed by scanning electron microscopy, X-ray diffraction and Vickers microhardness testing. The kinetic activity of boronized layers growth obeys the parabolic law, and the maximum thickness was 182 ± 10 µm. The thickness of FeB makes up to 40% of the total layer thickness. The obtained layers have two phases, which were composed of FeB and Fe_2B phases, except for the sample boronized at 1173 K for 1 h which had an Fe_2B layer only. The microhardness of the Fe_2B phase had a range of 1370–1703 $HV_{0.1}$, and that of the FeB phase was within 1727–2231 $HV_{0.1}$. During the boronizing process, the chromium created extra particles with the highest amount of chromium in the transient region. The highest amount of silicon was observed at the boride layer/substrate interface. The amount of manganese was slightly lower in the boride layers compared to the amount in the substrate. Finally, the integral diffusion model was applied to determine the boron activation energies in the FeB and Fe_2B layers, and this was followed by a comparison with the literature data.

Keywords: Royalloy steel; boronizing; boride layers; microstructure; integral diffusion model

check for updates

Citation: Orihel, P.; Drienovský, M.; Gabalcová, Z.; Jurči, P.; Keddam, M. Characterization and Boron Diffusion Kinetics on the Surface-Hardened Layers of Royalloy Steel. *Coatings* **2023**, *13*, 113. https://doi.org/10.3390/coatings13010113

Academic Editor: Engang Fu

Received: 2 December 2022
Revised: 2 January 2023
Accepted: 4 January 2023
Published: 7 January 2023

Copyright: © 2023 by the authors. Licensee MDPI, Basel, Switzerland. This article is an open access article distributed under the terms and conditions of the Creative Commons Attribution (CC BY) license (https://creativecommons.org/licenses/by/4.0/).

1. Introduction

Boronizing is a thermo-chemical process in which the boron atoms are introduced into the metallic surfaces, especially steels. This process is usually realized at the temperature range of 1023–1323 K for 0.5–10 h. During boronizing, the layers with high microhardness, good corrosion and wear resistance, low friction coefficient and good adhesion to the substrate are formed.

The boronizing process can be carried out in gases [1,2], liquids [3], solids (paste or powder) [4,5], plasmas [6] or by electrolysis [7]. After the boronizing process, the materials can be either air-cooled or re-austenitized, then, rapidly cooled in a quenching medium and tempered to achieve the suitable desired balance between the strength and the toughness [8].

In practice, the most widespread process is powder boronizing since it is simple and inexpensive [9]. However, plasma- or electrolytic boronizing makes it possible to shorten the duration of processes and to lower the processing temperatures [10].

In case of carbon steels, the formation of boride layers follows the iron–boron equilibrium diagram [11]. As per this diagram, two phases (FeB and Fe_2B) are formed in this system. First, the Fe_2B phase (8.83 wt.% B) is obtained. This phase crystallizes in tetragonal crystal lattice, and its hardness value is around 1600 HV. The thermal expansion coefficient of Fe_2B phase is 281 × 10^{-6} K^{-1}. The FeB layer appears on the top surface, underneath the Fe_2B layer. This phase contains 16.23 wt.% B, and it crystallizes in an orthorhombic crystal lattice. The typical hardness value of this phase is around 2000 HV. The thermal expansion coefficient of this phase is 296 × 10^{-6} K^{-1}.

Boride layers can be two phased, composed of FeB + Fe_2B phases, or mono-phased, containing the Fe_2B phase only [10]. Because of there being great differences between the thermal expansion coefficients between the borides, cracking can occur at their interfaces. For this reason, mono-phased Fe_2B layers are preferred in most industrial applications [12]. In the case of carbon steels, the formation of an Fe_2B layer can be achieved by the application of a diffusion annealing process after boronizing or by a carefully controlling the boronizing parameters [13]. On the other hand, it is very difficult to obtain mono-phase Fe_2B layers in the case of high alloy steels because alloying elements foster the formation of FeB, and its thickness can make up to 50% of the total layer thickness [14,15]. Moreover, borides of alloying elements, especially chromium borides (Cr_xB_y), may also occur in the boride layers formed on the surfaces of highly alloyed steels [16].

The total thickness of the boride layers increases as both the boronizing temperature and duration increase. The maximum total thickness of the boronized layers formed on pure iron [2,17] or low-carbon steels [18] can reach up to 0.4 mm. However, increasing the carbon and alloying elements content inhibits the growth of the boride layers [19,20]. This is because the carbon and alloying elements decrease the active diffusion in boron in iron-based solid solutions. In the cases of pure iron, low- and medium-carbon steels, the borides/substrate interface morphology is typically classified as a "sawtooth" one [2,17]. By increasing the content of both the carbon and alloying elements [12,13,19–21], the "sawtooth" morphology becomes disturbed, and the interface is flattened. In addition, the presence of large amounts of chromium in steels promotes the formation of FeB rather than Fe_2B, hence, the thickness of the FeB makes up around 50% of the total layer thickness developed on the high-chromium steels [14,22]. Silicon is another important element that is present in certain amounts in most steels. Silicon is a strong ferritizer, and it is insoluble in borides [23,24]. Therefore, Si atoms are pushed to the substrate region close to the borides where they stabilize the ferrite, which may further inhibit the layer growth.

The FeB- and Fe_2B compounds are different in terms of their hardness. The hardness of Fe_2B normally ranges between 1400 and 1750 HV, and it is almost independent of the carbon- and alloying elements content [2,12,13]. The hardness of FeB is much higher than that of Fe_2B, and its values often exceed 2000 HV for plain carbon steels [2]. As reported by Kayali and Taktak [25] or Keddam et al. [12], the hardness of FeB is marginally higher when Cr and Cr-V ledeburitic tool steels are boronized. On the other hand, iron–boron compounds are very brittle; the Fe_2B layer manifests the fracture toughness in the range of 5–6 $MPa.m^{1/2}$ [26,27], and FeB is even more brittle, as demonstrated by Uslu et al. for instance [28].

Over the last period, mathematical approaches have gained a great importance in the selection of the appropriate layer thicknesses of boride coatings for industrial applications. There are some published studies on the utilization of kinetic analyses of boronizing of high chromium ledeburitic tool steels. Gunes and Kanat [29], for instance, focused on the kinetic analysis of pack boronized (in the range of 1123–1323 K) AISI D6 steel. The obtained layers were double phased, and they were composed of FeB and Fe_2B. The measured total boride layer thickness ranged from 13.54 μm to 164.42 μm, and the boron activation energy was 180.36 kJ mol^{-1}. In another work, Sen et al. [30] boronized the AISI D2 steel in a salt bath and arrived to an activation energy for the boride layer of 170 kJ mol^{-1}. More recently, Keddam and Kulka [31] boronized the same steel grade in a powder. They have found that powder boronizing requires more activation energy than salt bath boronizing does (around 200 vs. 170 kJ mol^{-1}, respectively) to produce the borides at the surface.

To date, however, no relevant study has been conducted on the boronizing of high-chromium tool steel that contains only a very small amount of carbon. To overcome this gap in knowledge, we selected the plastic mould steel Uddeholm Royalloy (0.05 wt.% C, 12.6 wt.% Cr) as a model material.

This paper deals with the basic characteristics of boronized layers that are developed on a low-carbon high-chromium steel substrate. The generated layers were examined by SEM to reveal their microstructure, the morphology of the borides/substrate interfaces and

to measure their thicknesses. The elemental distribution was obtained via EDS mapping. The contents of Cr in each individual boron compound and the Si contents in the transient zones were determined for selected boronizing parameters by point EDS analyses. The XRD analysis was performed to identify the boride phases at the surfaces of the treated samples. The microhardness values were obtained in each zone to explain the influence of boronizing on the surface features of the Royalloy steel. The microstructures, the thickness of each individual boronized region, the alloying element redistribution between the borides and substrate, the phase composition of the boride layers and their microhardness are described and discussed. Finally, the integral diffusion model as a recent kinetic approach [32] was utilized to assess the boron diffusion coefficients in the iron boride layers (FeB and Fe_2B). This kinetic approach assumed a parabolic distribution of boron elements across the double boride layer (FeB+ Fe_2B). The values of the activation energies in FeB and Fe_2B were deduced, and the results are discussed based on the literature data.

2. The Integral Diffusion Model

2.1. Mathematical Foundation of the Applied Kinetic Modelling

The integral method [32] recently utilized for describing the kinetics of the bilayer (FeB/Fe_2B) generated at the surface of 34CrAlNi7 steel was applied for the case of pack-boronized Royalloy steel. Figure 1 presents a schematic boron distribution profile across the bilayer (Fe_2B/FeB) with no occurrence of boride incubation periods.

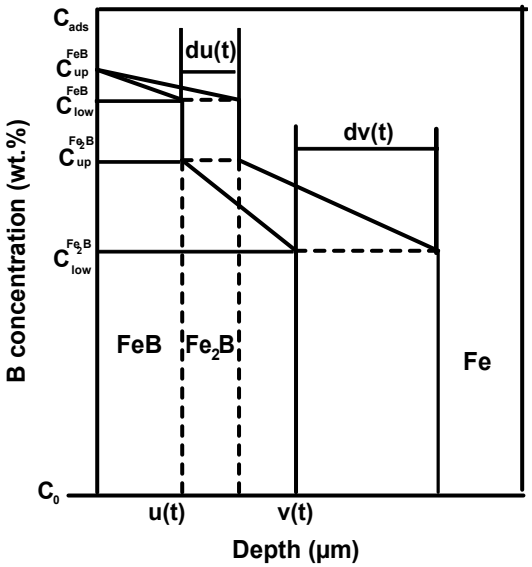


Figure 1. Schematic distribution of boron concentration within the bilayer (FeB/Fe_2B).

In Figure 1, the values of the maximum and minimum concentrations in FeB are the following: C_{up}^{FeB} (=16.40 wt.% B) and C_{low}^{FeB} (=16.23 wt.% B), respectively. In case of diiron boride (Fe_2B), its maximum and minimum concentrations are expressed as $C_{up}^{Fe_2B}$ (=9 wt.% B) and $C_{low}^{Fe_2B}$ (=8.83 wt.% B), respectively [33,34]. The boron concentration C_{ads} designates the adsorbed quantity at the material surface as defined by Yu et al. [35]. $u(t)$ refers to the FeB layer thickness, and $v(t)$ is that of the bilayer (FeB/Fe_2B). C_0 represents the concentration of boron atoms within the substrate, whose value is very low [11,36]. The initial and boundary conditions employed for solving this diffusion-controlled problem can be found elsewhere; see [32–34] for more details. Consequently, the assessment of the boron diffusion coefficients in FeB and Fe_2B requires the numerical resolution of a system of nonlinear equations derived from the following set of differential algebraic Equations (1)–(6) (DAE).

$$a_1(t)u(t) + b_1(t)u(t)^2 = (C_{up}^{FeB} - C_{low}^{FeB}) \quad (1)$$

$$a_2(t)[v(t) - u(t)] + b_2(t)[v(t) - u(t)]^2 = (C_{up}^{Fe_2B} - C_{low}^{Fe_2B}) \quad (2)$$

$$\frac{d}{dt}[\frac{u(t)^2}{2}a_1(t) + \frac{u(t)^3}{3}b_1(t)] = 2D_{FeB}b_1(t)u(t) \quad (3)$$

$$2w_{12}\frac{dv(t)}{dt} + \frac{[v(t)-u(t)]^2}{2}\frac{da_2(t)}{dt} + \frac{[v(t)-u(t)]^3}{3}\frac{db_2(t)}{dt} = 2D_{Fe_2B}b_2(t)[v(t)-u(t)] \quad (4)$$

$$[a_1^2(t) - 2w_1b_1(t)]D_{FeB} = a_1(t)[a_2(t) + 2b_2(t)(v(t)-u(t))]D_{Fe_2B} \quad (5)$$

$$2w_{12}a_2(t)b_1(t)D_{FeB} = a_1(t)[a_2^2(t) - 2w_2b_2(t)]D_{Fe_2B} \quad (6)$$

with

$$w_1 = [\frac{(C_{up}^{FeB} + C_{low}^{FeB})}{2} - C_{up}^{Fe_2B}]\ w_2 = [\frac{(C_{up}^{Fe_2B} + C_{low}^{Fe_2B})}{2} - C_0]$$

and

$$w_{12} = \frac{(C_{up}^{Fe_2B} - C_{low}^{Fe_2B})}{2}$$

$$u(t) = 2\varepsilon\sqrt{D_{FeB}t} = k'\sqrt{t} \quad (7)$$

$$v(t) = 2\eta\sqrt{D_{Fe_2B}t} = k\sqrt{t} \quad (8)$$

2.2. Derivation of Expressions of Boron Diffusion Coefficents in FeB and Fe_2B

By considering Equations (7) and (8) for the layers' thicknesses, the obtained set of nonlinear equations [32,33] can be solved numerically with the aid of Newton–Raphson routine [37] to find the α_1, α_2,β_1 and β_2 values, as well as the two dimensionless parameters ε and η. Finally, the values of boron diffusion coefficients of boron in the iron borides can be derived from Equations (9) and (10):

$$D_{FeB} = (\frac{k'}{2\varepsilon})^2 \quad (9)$$

$$D_{Fe_2B} = (\frac{k}{2\eta})^2 \quad (10)$$

$$\text{with } \varepsilon = \sqrt{\frac{\beta_1}{(\frac{\alpha_1}{2} + \frac{\beta_1}{3})}} \text{and } \eta = k\sqrt{\frac{\beta_2}{[2w_{12}k(k-k') - (\frac{\alpha_2}{2} + \frac{2\beta_2}{3})(k-k')^2]}}$$

The two parameters k' and k represent the parabolic growth constants at the two interfaces (FeB/Fe_2B) and (Fe_2B/substrate), respectively. Their values can be deduced empirically from the slopes of the straight lines relating $u(t)$ and $v(t)$ to the square root of the treatment time.

3. Material and Experimental Techniques

The analyzed material was low-carbon high-chromium Royalloy steel with a chemical composition (in wt.%) of 0.05% C, 0.4% Si, 1.2% Mn, 12.6% Cr and Fe, which were balance. A total of 51 samples were made from this steel. Prior to boronizing, the samples were subjected to the metallographic preparation, which consisted of grinding by SiC sandpapers (600 grit and 1200 grit), and subsequently polishing them using a diamond paste with particle sizes of 6, 3 and 1 μm. After that, the samples were ultrasonically cleaned and degreased in acetone for 15 minutes. Then, they were placed into the container that is shown in Figure 2, which was filled with Durborid powder mixture. The container was hermetically sealed and inserted into an electrical resistance furnace where it was heated to the pre-determined boronizing temperature. The boronizing process was carried out at 1173, 1223, 1248, 1273 or 1323 K for 1, 3, 5, 7 or 10 h for each temperature test. After the boronizing process, the samples were slowly cooled down to the room temperature, removed from the container and cleaned of the boronizing powder.

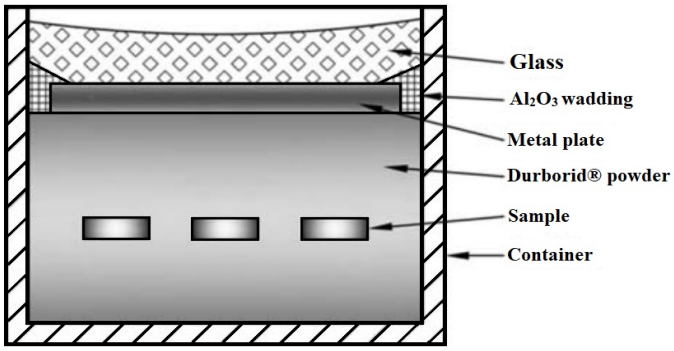


Figure 2. Container with its components used for pack boronizing of Royalloy steel.

Cross-sectioned metallographic specimens were subjected to the standard metallographic preparation line. After the final step of polishing, the samples were etched in COR etchant (CH_3COOH; HCL; picric acid, CH_3OH) for 5–7 s. The microstructures were analyzed using a scanning electron microscope (SEM) Jeol JSM-7600F using a secondary electrons (SE) detection regime at an acceleration voltage of 15 kV. The thickness of the individual boride layers was estimated using randomly selected SEM cross-sectional images at an appropriate magnification. To obtain a sufficient reliability of the obtained results, an approach by Kunst and Schaaber [38] was used. For a more precise determination of the chemical elements' redistribution during the boronizing process, energy dispersive spectroscopy (EDS) was used, where the point analysis (a min. of 8 measurements in each boride compound, and of the newly formed particles in transient region and substrate) and chemical elements mapping were realized.

Results from XRD analysis of all of the boronized samples were obtained using a PANalytical Empyrean X-ray diffractometer (XRD) (Malvern Panalytical Ltd., Malvern, UK) with $Co_{K\alpha 1,2}$ characteristic radiation, which were filtered by Fe. The results were recorded in the 2-theta angle, and they had a range of 30–100°, with a step of 0.05°. The incident beam was modified by a 0.04 rad soller slit, a $\frac{1}{4}°$ divergence slit and a $\frac{1}{2}°$ anti-scatter slit. The diffracted beam path was equipped with a $\frac{1}{2}°$ anti-scatter slit, a 0.04 rad soller slit, an Ni beta filter and a PIXcel3D position sensitive detector which was operated in the 1D scanning mode. At this point, it should be noted that the recorded results also represent the phase composition of the substrate because of the penetration depth of the X-rays. The identification of peaks was made using the PANalytical Xpert High Score program (HighScore Plus version 3.0.5) with the ICSD FIZ Karlsruhe database.

The microhardness values of the borides and diffusion zone were measured using a Hanneman hardness tester using a HV 0.1 (100 g) load and 15 s loading time. Seven measurements were taken in each place and in each specimen to obtain the relevant information about the Vickers microhardness. Then, the mean values and statistical uncertainties were calculated from the obtained microhardness values.

The results of the phase equilibria calculation (simulation) were performed using Thermo-Calc, version 2022. A commercially available database for steels/Fe-alloys, version 9.3 (TCFE9), was employed. Both the Thermo-Calc and the database are software products of the Thermo-Calc Software company, which is based in Solna, Sweden. The calculation itself consisted of three steps: The first one is a system definer, where the chemical composition of the alloy was given. It was followed by the second step, an equilibrium calculator, where all of the calculations were performed, and the last step was a plot renderer, where the final plot was adjusted by the end user.

4. Results and Discussions

4.1. Microstructural Exmainations

To examine the microstructures, we performed SEM observations of the morphology of the borides/substrate interfaces. To follow the redistribution of the alloying elements

between the boron compounds and the substrate, the EDS mapping of the main elements was also carried out. Particularly, the change in the contents of Cr and Si with the process parameters was investigated from quantitative point of view.

Characteristic microstructures of differently boronized specimens in cross-sectional SEM micrographs are shown in Figure 3. It is seen that almost all of the boride layers had two phases, which were composed of FeB and Fe_2B phases, except for the samples boronized at 1173 K for 1 h with a single-phase (Fe_2B) layer. Below the borides, a region with an enhanced number and population density of extra particles can be seen.

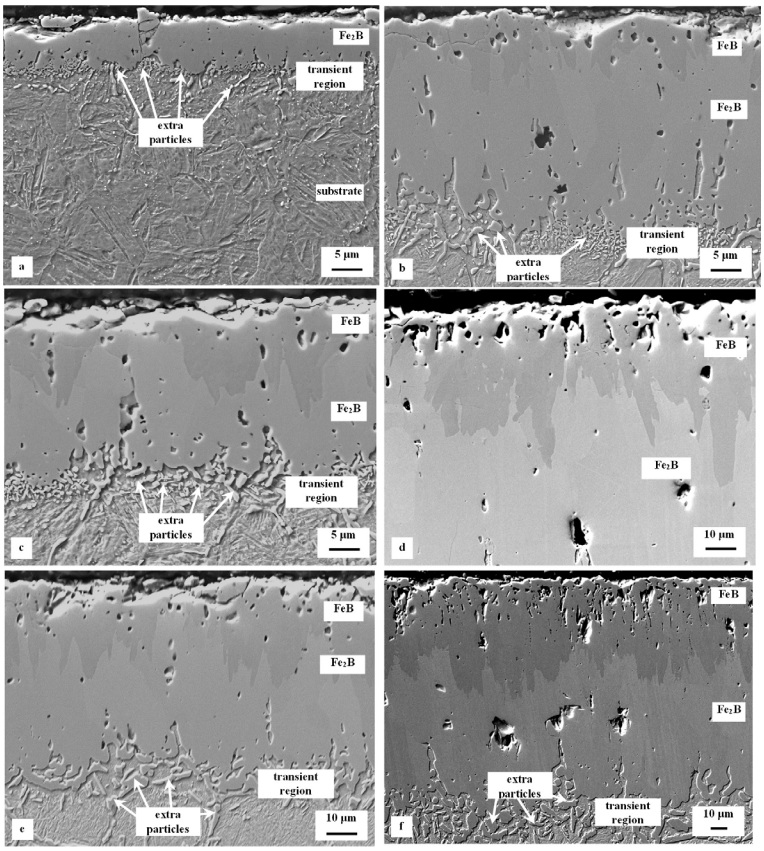


Figure 3. Cross sectional SEM images of samples boronized at different process parameters: (**a**) 1173 K for 1 h, (**b**) 1173 K for 10 h, (**c**) 1248 K for 1 h, (**d**) 1248 K for 10 h, (**e**) 1323 K for 1 h and (**f**) 1323 K for 10 h.

An example of EDS maps of Royalloy steel (sample boronized at 1173 K for 10 h) is shown in Figure 4. It is clearly visible that a significant redistribution of alloying elements took place during the boronizing process. The chromium atoms are accumulated in extra particles in thin region underneath the borides, however, the crystallography of these particles is not clear yet. Silicon does not assist in borides formation since it is completely insoluble in them [23]. Most of the Si is gathered in a solid solution close to the Fe_2B/substrate interface, with maximum concentrations above 4 wt.%. This finding is consistent with recent results published by Domínguez et al., who boronized a steel with a chemical composition of (in wt.%) 0.1% C, 0.20% Si, 0.85% Mn, 0.20% Cu, 0.040% P and 0.050% S [24]. In this paper, it was reported that silicon was expelled from the surface by growing borides nearby to the Fe_2B/substrate interface, and resulting in the formation of Fe-Si-B compounds ($FeSi_{0.4}B_{0.6}$ and Fe_5SiB_2). Manganese was pushed out of the boride layers during the boriding process, and the highest content of this element was found in the particles within the transient region.

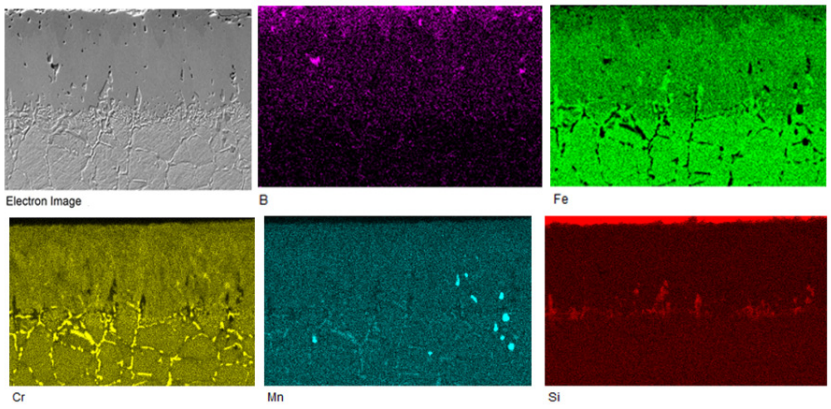


Figure 4. SEM pictures and EDS maps of chemical elements in the sample boronized at 1173 K for 10 h.

The boride layers contain slightly larger amount of chromium compared with the substrate (Figure 5). This proves that chromium is transported from the substrate to the borides during the boronizing process, making the adjacent region beneath the boride layers depleted of it. Another interesting finding is that the Fe_2B phase contains a slightly higher chromium content value compared to that of the FeB phase. The cause of this phenomenon may be the gradual diffusion of chromium from the substrate into the boride layers or its easier incorporation into the Fe_2B phase compared with that of the FeB phase. The newly formed particles in the transient region contain in all of the cases with the highest amount of chromium of around 20–30 wt.%. As already mentioned, the highest amount of silicon was found in the transient region underneath the boride layers. The maximum amount of silicon in this area ranged between 2.4 and 4.54 wt.% (Figure 6), and it increased as the boronizing temperature increased.

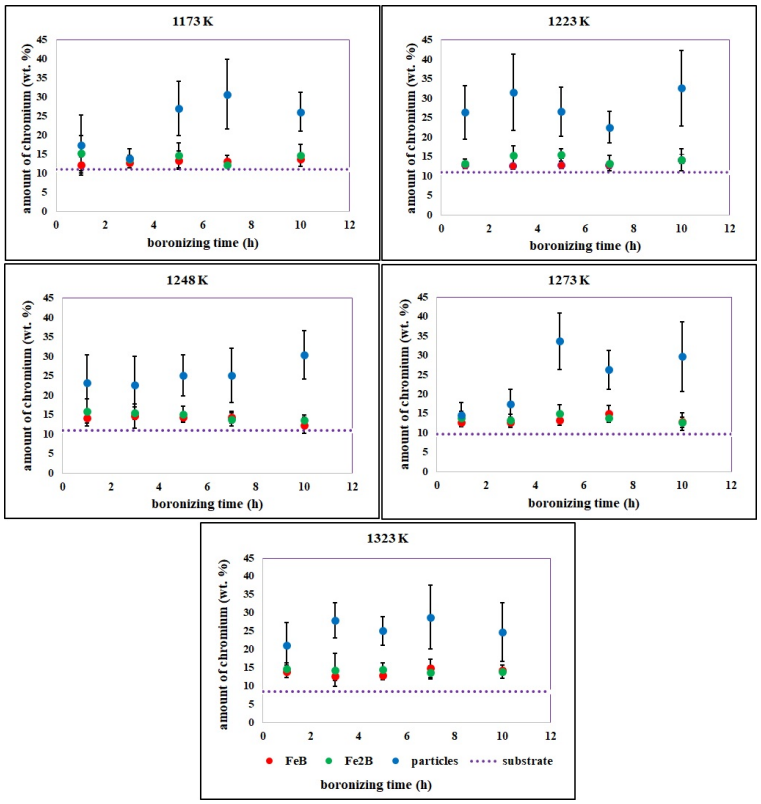


Figure 5. Chromium contents in FeB, Fe_2B and particles underneath the boride layers and substrate.

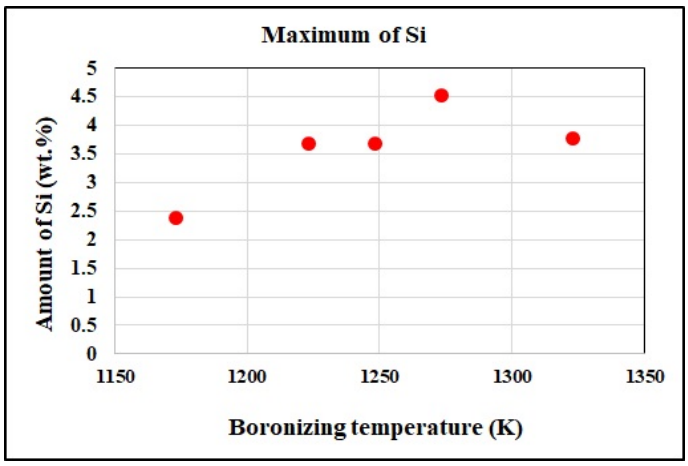


Figure 6. Maximum value of silicon content in the transient region underneath the boride layers for differently boronized specimens.

4.2. XRD Analysis

It is well recognized that the chemical composition of boriding agent in the powdered method influences the phase constitution of generated, boronized layers on steel surfaces. Therefore, the purpose of carrying out the XRD analyses is to prove the presence of iron borides, and eventually, the alloying elements of borides as precipitates inside the boronized layers.

The XRD patterns of the samples boronized at 1173, 1248 and 1323 K for 1 or 10 h are shown in Figure 7. The XRD analysis proved that all of the boride layers have two phases, which are composed of FeB and Fe_2B phases, except for sample boronized at 1173 K for 1 hour. No presence of borides of alloying elements were detected. This finding is rather inconsistent with observations of various investigators who have identified borides of alloying elements in the boronized layers in highly alloyed steels. For instance, chromium and manganese borides were found in powder-boronized AISI 440C steel (2.1 wt.% C; 16.50 wt.% Cr; 0.417 wt.% Mn) [9]. The presence of CrB, Cr_2B and MoB was reported by Erdogan and Gunes for boronized steel with a chemical composition of (in wt.%) 0.90 %C, 7.80 %Cr and 2.50 %Mo [11]. In another study, Boumaali et al. [39] pack boronized the AISI H13 steel containing 5.25 wt.% Cr, 1.65 wt.% Mo and 1 wt.% Si, and they identified the presence of VB and Cr_5B_3 phases besides the iron borides (FeB and Fe_2B) on the surfaces of the treated samples at 1273 K for 2, 4 and 6 h.

Contrarily, no presence of chromium borides was found on the surfaces of powder-boronized Vanadis 6 steel [12]. The great discrepancy in the obtained results might exist because the characteristic peaks of chromium borides Cr_xB_y and iron borides can overlap. Additionally, chromium borides can form small particles embedded in iron borides, which makes it very difficult to identify them by XRD. However, this issue requires further careful investigation, and a conclusive statement will be achievable only by applying transmission electron microscopy to investigation of the sub-structure of borides.

4.3. Microhardness Measurements

To investigate the effect of the boronizing treatment on the surfaces of the treated samples, microhardness measurements were taken cross-sectionally in each characteristic boron compound and in a transient zone.

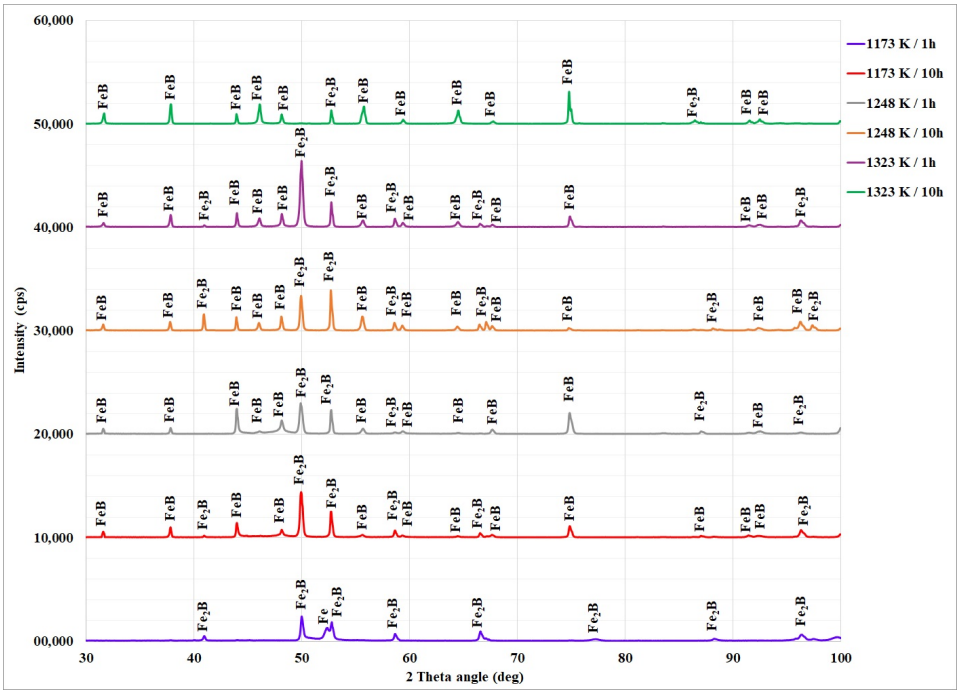


Figure 7. X-ray diffraction patterns obtained on the surfaces of boronized Royalloy steels at different process parameters.

The mean values of microhardness of the differently boronized specimens are shown in Figure 8. Generally, FeB manifested higher microhardness values in the range of 1727–2231 HV 0.1. The diffusion zone manifested the lowest microhardness values among the analysed regions, and the values were around 500 HV 0.1. The microhardness values of the Fe_2B phase were in range of 1370–1703 HV 0.1. The obtained microhardness values in all three characteristic regions are practically independent on the boronizing strategies used in the current work. Compred with the outcomes obtained by other investigators, no significant deviations were detected. Keddam et al. [12] established very similar microhardness values in the boronized layers of Vanadis 6 steel. Kayali and Taktak [25] boronized Cr-containing steels, and they also found very similar findings. One can thus suggest that the substrate chemistry has only a minimal impact on the resulting microhardness of the obtained borides.

4.4. Kinetic Analysis with the Integral Method

The analysis of the kinetics data makes it possible to study the time evolution of the layers' thicknesses and to determine the values of the activation energies that allow the diffusion of boron atoms to occur during the pack boronizing of Royalloy steel. It is understood that the change in the growth rate of iron borides is directly linked to the relative mobility of boron atoms in each iron boride (FeB or Fe_2B). Consequently, the experimental determination of the parabolic growth constant values at the two interfaces permits us to make an assessment of the boron diffusion coefficients in FeB and Fe_2B by using the integral diffusion model [32].

The thicknesses of individual boride layers were measured at five randomly selected places on the SEM images at an appropriate magnification. Figure 9 gives the experimental layers' thicknesses of FeB and (FeB + Fe_2B) as a function of the square root of the treatment time, and we fitted the data with Equations (7) and (8) at five different temperatures. As we can see in Figure 9, the thickness of the boride layers increases depending on the boronizing parameters.

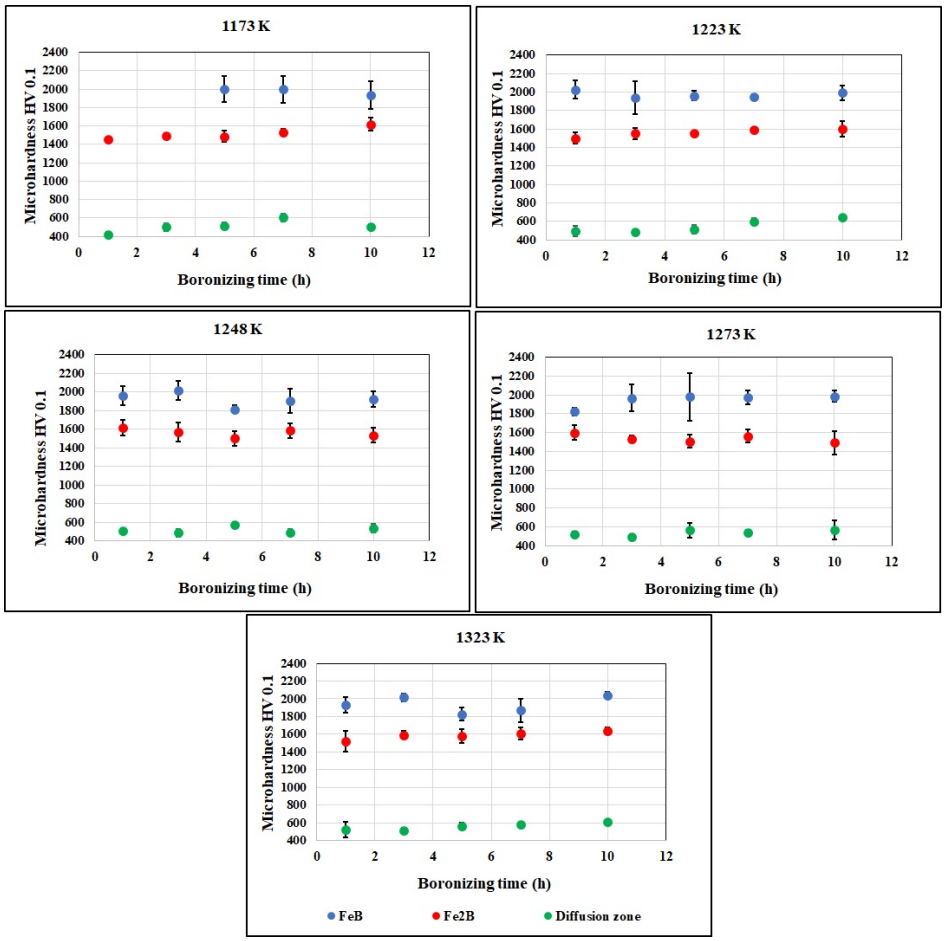


Figure 8. Vickers microhardness of FeB, Fe_2B layers and diffusion zone measured for Royalloy steel treated at different temperatures.

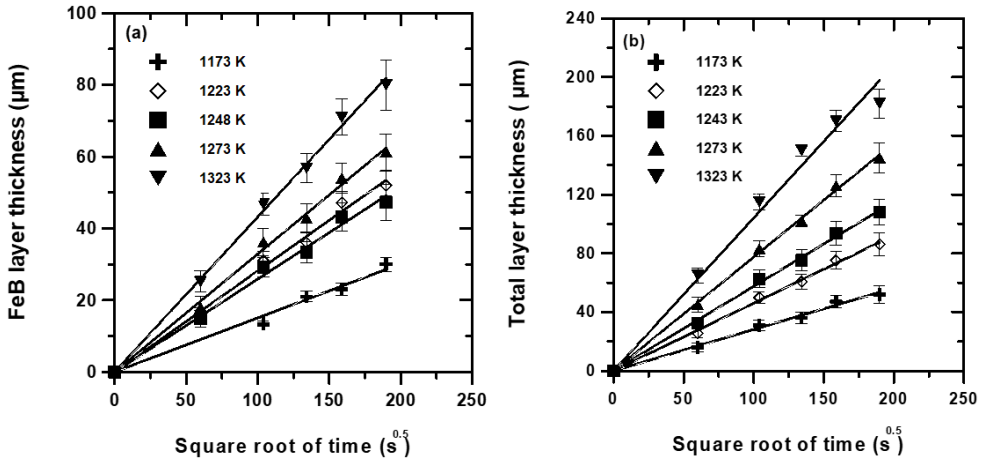


Figure 9. Time dependence of layers' thicknesses for five temperatures: (**a**) FeB layer; (**b**) (FeB + Fe_2B).

The obtained straight lines show a controlled diffusion process, conforming to a parabolic growth law for the given boronizing conditions. However, some deviations from the parabolic thickness–duration relationship can be observed in the boronizing treatment with the presence of alloying elements in the substrate. A probable reason for this phenomenon can be the redistribution of alloying elements during boronizing process (Figures 4–6), especially the redistribution of silicon, which is accumulated at the boride

layers/substrate interfaces. As already mentioned, the alloying elements decreased the flux of active boron atoms into the substrate.

Moreover, silicon is a strong ferrite stabilizer [40]. The solubility of boron in ferrite is very low, so the presence of the ferrite can inhibit the boride layers growth. To confirm or refute this theory, the Thermo-calc simulation of the phase equilibria for the maximum Si content below the borides was performed. The results are shown in Figure 10. The presence of either a BCC phase (ferrite) or BCC/FCC mixtures at low carbon contents are clearly visible, hence the stabilization of ferrite is highly probable during the boronizing of Royalloy steel, and it can explain small deviations in the boride layers growth kinetics from the parabolic law.

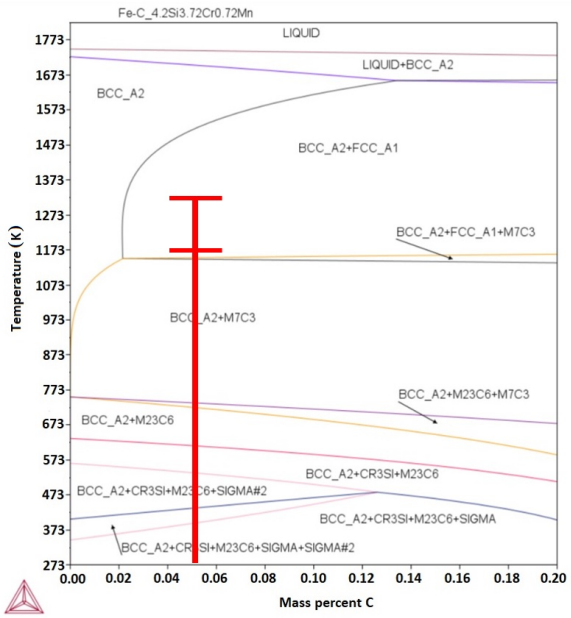


Figure 10. Result of Thermo-calc simulation of phase equilibria for 4.2% Si, 3.72% Cr and 0.72% Mn (maximum determined Si content below the borides). BCC—ferrite; FCC—austenite; other phases are carbides and sigma phase. The range of boronizing temperatures used in the current work is indicated by two horizontal red lines. Vertical line indicates the actual carbon content in examined steel.

In Table 1, the experimental data are presented regarding the values of the experimental parabolic growth constants at the two considered interfaces. Such values represent the slopes of the straight lines displayed in Figure 9.

Table 1. Experimentally deduced values of parabolic constants at the two interfaces from Equations (7) and (8).

T (K)	k' (μm s$^{-0.5}$)	k (μm s$^{-0.5}$)
1173	0.1506	0.2816
1223	0.2592	0.4609
1248	0.3282	0.5757
1273	0.4321	0.7748
1323	0.6219	1.0416

In Table 2, the assessed values of the boron diffusion coefficients in FeB and Fe_2B after we used the integral method are grouped. The numerically determined values of the two dimensionless parameters ε and η are nearly constant whatever the boriding temperature is due to the parabolic nature of the growth law for the boronized layers.

Table 2. Estimated boron diffusivities in FeB and Fe_2B based on the integral method.

T (K)	$D_{FeB} \times 10^{-12}$ ($m^2 s^{-1}$)	$D_{Fe_2B} \times 10^{-12}$ ($m^2 s^{-1}$)	ε Parameter	η Parameter
1173	1.12	0.75	0.07093	0.1617
1223	3.29	1.94	0.07185	0.1653
1248	5.18	2.99	0.07207	0.1663
1273	9.08	5.54	0.07188	0.1646
1323	18.20	9.35	0.07288	0.1703

Figure 11 provides the plot of fitted natural logarithms of estimated boron diffusivities in iron borides according to the Arrhenius relationships. The results of this fitting are given in the form of Equations (11) and (12):

$$D_{FeB} = 7.54 \times 10^{-2} \exp\left(-\frac{242.79}{RT}\right) \quad (11)$$

$$D_{Fe_2B} = 6.59 \times 10^{-3} \exp\left(-\frac{223.00}{RT}\right) \quad (12)$$

in which R is the ideal gas constant (=8.314 J mol^{-1} K^{-1}), and T the boronizing temperature, which is given in Kelvin.

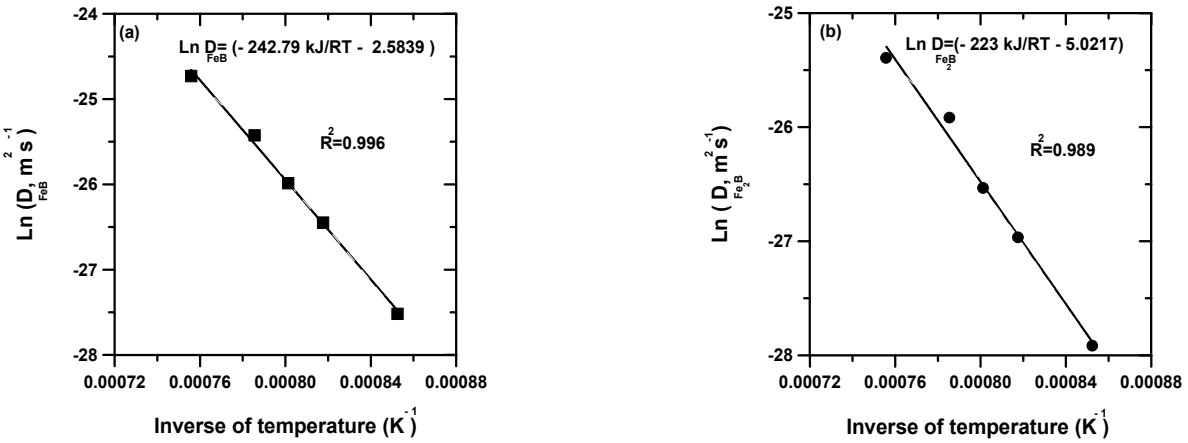


Figure 11. Change in the temperature of the natural logarithm of estimated boron diffusivities in both borides: (**a**) FeB and (**b**) Fe_2B.

In Table 3, the values of the boron activation energies are listed [30,31,33,41–47] for boronized steels taken from the literature together with the values found in the present work. It is clearly obvious that the reported values of the activation energies are influenced by several factors, which are summarized as follows: the chemical composition of the treated substrates, the boronizing method, the chemical composition of the boron source, the process parameters selected, the nature of the chemical or electrochemical reactions involved, the overactivation of the boron diffusion process and the computation method. We should mention that the computation methods include the applied diffusion models [31,33,42,44,47] for the boronizing kinetics on various substrates of steels and the empirical approach using the classical parabolic growth law [30,41,43,45,46]. From Table 3, it can be noticed that the found value of the boron activation energy for AISI 316 steel [46] was lower than the values of the energies obtained from the powder pack boriding [31,33,41–44] or liquid boriding [30], owing to the difference in the diffusion rates of the boron atoms. Türkmen et al. [44] used an alternative boron source (boric acid) in the powder mixture instead of the usual boron compound (boron carbide) to thermochemically

treat SAE 1020 steel. Thus, the use of the powder mixture composed of 22.5 wt.% H_3BO_3, 5 wt.% KBF_4 and 72.5 wt.% SiC resulted in a single monolayer of the Fe_2B type on SAE 1020 steel [44].

Table 3. Confrontation of the calculated boron activation energies with the literature data.

Steel	Boronizing Method	Temperature Range (K)	Activation Energy ($kJmol^{-1}$)	Computation Method	Refs.
AISI 316	Powder	1073–1273 for 1–3 h	172.93 (FeB) 199.43 (Fe_2B)	Integral method	[33]
ASP®2012	Powder	1123–1223 for 2–6 h	314.716 (FeB + (Fe_2B)	Parabolic law	[41]
AISI M2	Powder	1173–1323 for 4–10 h	226.02 (FeB) 209.04 (Fe_2B)	Dybkov model	[42]
AISI D2	Powder	1223–1273 for 3–10 h	208.04(FeB) 197.46 (Fe_2B)	Mean diffusion coefficient method	[31]
Hardox-450	Powder	1123–1223 for 2–6 h	157.99 (Fe_2B)	Parabolic law	[43]
SAE 1020	Powder	1123–1223 for 4–12 h	183.14 (Fe_2B)	Integral method	[44]
AISI D2	Salt bath	1073–1273 for 2–8 h	170 (FeB + Fe_2B)	Parabolic law	[30]
AISI 304	CRTD-Bor	1223–1323 for 0.25–1 h	181.46 (Fe_2B)	Parabolic law	[45]
AISI 316	Plasma-paste-boriding	973–1073 for 3–7 h	118.12 (FeB + Fe_2B)	Parabolic law	[46]
AISI 316 L	Pulsed DC powder	1123–1273 for 0.5–2 h	162 (FeB) 171 (Fe_2B)	Diffusion model	[47]
Royalloy	Powder	1173–1323 for 1–10 h	242.79 (FeB) 223.0 (Fe_2B)	Integral method	This work

It is concluded that the derived values of boron activation energies from the present study are consistent with the empirical expectations and comparable to those in [31,33,41,42], which are displayed in Table 3, when we were utilizing the powder method. In terms of the limitations of the current kinetic approach, which is named the integral method, the effect of metal borides precipitation as chromium borides within the dual boride layer was not examined. This situation could greatly influence the diffusion rate of boron atoms by slowing down its mass flux. In addition, even though the value of the carbon content (=0.05 wt.%) in the Royalloy steel was low, it could impact the diffusion process of boron on an atomic scale.

5. Conclusions

In this work, the Royalloy steel was pack boronized in the temperature range of 1173–1323 K for 1–10 h. The main concluding points can be presented as follows:

Dual-phase boride layers were generated for most of the treatment strategies, except for the combinations of low temperatures and a 1 h duration.

The maximum thickness of the entire boride layer (FeB +Fe_2B) was 182 ± 10 μm. The thickness of FeB makes up to 40% of the total thickness.

A considerable redistribution of alloying elements throughout the borides and the adjacent region was detected. Borides contain more chromium than the substrate does. In close to borides the region close to the borides, extra particles with 20–30 wt.% Cr formed. Silicon was pushed from the growing borides, and it was gathered in a thin

region close to the borides/substrate interface, with the maximum amount ranged between 2.4 and 4.54 wt.%.

The Vickers microhardness of the FeB phase was in the range of 1727–2231 $HV_{0.1}$, while that of Fe_2B was between 1370 and 1703 $HV_{0.1}$. No strong dependence was observed between the microhardness of the boride layers and the boronizing parameters.

The estimated activation energies for boron diffusion in FeB and Fe_2B were, respectively, 242.79 and 223.0 $kJmol^{-1}$ when we were using the integral diffusion model. The assessed results in terms of activation energies were in line with the literature results.

As a main limitation, the integral method overlooked the possible influence of Cr borides' precipitates on the boron diffusion during the generation of dual boride layers on the Royalloy steel. However, the presence of these borides should be verified in further investigations.

Author Contributions: Conceptualization, M.K. and P.J.; Formal Analysis, M.K. and P.J.; Investigation, P.O., Z.G., M.D. and M.K.; Methodology, M.K. and P.J.; Supervision, M.K. and P.J.; Validation, P.O., M.K. and P.J.; P.O., M.D., and M.K.; Writing—Original Draft, M.K., P.O. and P.J.; Writing—Review and Editing, M.K. and P.J. All authors have read and agreed to the published version of the manuscript.

Funding: This research received funding from the project below. The project covered a part of wages of scientists from Faculty of Material Sciences and Technology of the STU in Trnava involved in the preparation of the manuscript. This work was co-funded by the European Regional Development Fund, project No. ITMS2014+: 313011W085.

Institutional Review Board Statement: Not applicable.

Informed Consent Statement: Not applicable.

Data Availability Statement: Not applicable.

Conflicts of Interest: The authors declare no conflict of interest.

References

1. Keddam, M.; Kulka, M.; Makuch, N.; Pertek, A.; Małdziński, L. A kinetic model for estimating the boron activation energies in the FeB and Fe2B layers during the gas-boriding of Armco iron: Effect of boride incubation times. *Appl. Surf. Sci.* **2014**, *298*, 155–163. [CrossRef]
2. Kulka, M.; Makuch, N.; Piasecki, A. Nanomechanical characterization and fracture toughness of FeB and Fe 2 B iron borides produced by gas boriding of Armco iron. *Surf. Coat. Technol.* **2017**, *325*, 515–532. [CrossRef]
3. Pham, N.T.H.; Nguyen, L.N.P.; Tam, H.T.T.A. A study of SiC/Borax liquid boride layer on AISI H13 hot work tool steel. *Int. J. Appl. Eng. Technol.* **2021**, *3*, 23–28.
4. García-León, R.A.; Martinez-Trinidad, J.; Campos-Silva, I.; Wong-Angel, W. Mechanical characterization of the AISI 316L alloy exposed to boriding process. *Dyna* **2020**, *87*, 34–41. [CrossRef]
5. Ipek, M.; Efe, G.C.; Ozbek, I.; Zeytin, S.; Bindal, C. Investigation of Boronizing Kinetics of AISI 51100 Steel. *J. Mater. Eng. Perform.* **2012**, *21*, 733–738. [CrossRef]
6. Gunes, I.; Ulker, S.; Taktak, S. Kinetics of plasma paste boronized AISI 8620 steel in borax paste mixtures. *Prot. Met. Phys. Chem. Surf.* **2013**, *49*, 567–573. [CrossRef]
7. Jiang, Y.; Bao, Y.; Wang, M. Kinetic Analysis of Additive on Plasma Electrolytic Boriding. *Coatings* **2017**, *7*, 61. [CrossRef]
8. Jurči, P.; Hudáková, M. Diffusion Boronizing of H11 Hot Work Tool Steel. *J. Mater. Eng. Perform.* **2011**, *20*, 1180–1187. [CrossRef]
9. Kayali, Y.; Gunes, I.; Ulu, S. Diffussion kinetics of borided AISI 52100 and AISI 440C steels. *Vacuum* **2012**, *86*, 1428–1434. [CrossRef]
10. Xie, F.; Cheng, J.; Wang, S. Effects and mechanisms of an alternating current field on pack boriding. *Vacuum* **2018**, *148*, 41–47. [CrossRef]
11. Krukovich, M.G.; Prusakov, B.A.; Sizov, I.S. The Equilibrium Diagram of 'Boron-Iron' Binary System. In *Plasticity of Boronized Layers*; Springer: Cham, Switzerland, 2016; Volume 237, pp. 23–38.
12. Keddam, M.; Hudáková, M.; Ptačinová, J.; Moravčík, R.; Gogola, P.; Gabalcová, Z.; Jurči, P. Characterization of boronized layers on Vanadis 6 tool steel. *Surf. Eng.* **2021**, *37*, 445–454. [CrossRef]
13. Campos-Silva, I.; Flores-Jiménez, M.; Rodríguez-Castro, G.; Hernández-Sánchez, E.; Martínez-Trinidad, J.; Tadeo-Rosas, R. Improved fracture toughness of boride coating developed with a diffusion annealing process. *Surf. Coat. Technol.* **2013**, *237*, 429–439. [CrossRef]
14. Dybkov, V.I. Boriding of High Chromium Steels. *Curr. Phys. Chem.* **2016**, *6*, 137–144. [CrossRef]
15. Dybkov, V.I. Basics of Formation of Iron Boride Coatings. *J. Miner.* **2016**, *2*, 30–46.

16. Dybkov, V.I.; Lengauer, W.; Barmak, K. Formation of Boride Layers at the Fe–10% Cr alloy–boron Interface. *J. Alloy. Compd.* **2005**, *398*, 113–122. [CrossRef]
17. Sireli, G.K.; Bora, A.S.; Timur, S. Evaluating the mechanical behavior of electrochemically borided low-carbon steel. *Surf. Coat. Technol.* **2020**, *381*, 125177. [CrossRef]
18. da Costa Aichholz, S.A.; Meruvia, M.S.; Júnior, P.C.S.; Torres, R.D. Tribocorrosion behavior of boronized AISI 4140 steel. *Surf. Coat. Technol.* **2018**, *352*, 265–272. [CrossRef]
19. Ozbek, I.; Bindal, C. Mechanical properties of boronized AISI W4 steel. *Surf. Coat. Technol.* **2002**, *154*, 14–20. [CrossRef]
20. Pereira, R.G.; Mariani, F.E.; Neto, A.L.; Totten, G.E.; Casteletti, L.C. Characterization of Layers Produced by Boriding and Boriding-PVD on AISI D2 Tool Steel. *Mater. Perform. Charact.* **2016**, *5*, 406–413. [CrossRef]
21. Erdogan, M.; Gunes, I. Corrosion Behavior and Microstructure of Borided Tool Steel. *Matéria* **2015**, *20*, 523–529. [CrossRef]
22. Oliveira, C.K.N.; Casteletti, L.C.; Lombardi Neto, A.; Totten, G.E.; Heck, S.C. Production and characterization of boride layers on AISI D2 tool steel. *Vacuum* **2010**, *84*, 792–796. [CrossRef]
23. Christiansen, T.L.; Bottoli, F.; Dahl, K.V.; Gammeltoft-Hansen, N.B.; Laursen, M.B.; Somers, M.A.J. Hard Surface Layers by Pack Boriding and Gaseous Thermo-Reactive Deposition and Diffusion Treatments. *Mater. Perform. Charact.* **2017**, *6*, 475–491. [CrossRef]
24. Ortiz-Domínguez, M.; Gómez-Vargas, O.A.; De Parga, G.A.; Torres-Santiago, G.; Velázquez-Mancilla, R.; Castellanos-Escamilla, V.A.; Mendoza-Camargo, J.; Trujillo-Sánchez, R. Modeling of the Growth Kinetics of Boride Layers in Powder-Pack Borided ASTM A36 Steel Based on Two Different Approaches. *Adv. Mater. Sci. Eng.* **2019**, *2019*, 5985617. [CrossRef]
25. Kayali, Y.; Taktak, S. Characterization and Rockwell-C adhesion properties of chromium-based borided steels. *J. Adhes. Sci. Technol.* **2015**, *29*, 2065–2075. [CrossRef]
26. Li, C.; Shen, B.; Li, G.; Yang, C. Effect of Boronizing Temperature and Time on Microstructure and Abrasion Wear Resistance of Cr12Mn2V2 High Chromium Cast Iron. *Surf. Coat. Technol.* **2008**, *202*, 5882–5886. [CrossRef]
27. Campos, I.; Farah, M.; López, N.; Bermúdez, G.; Rodríguez, G.; VillaVelázquez, C. Evaluation of the tool life and fracture toughness of cutting tools boronized by the paste boriding process. *Appl. Surf. Sci.* **2008**, *254*, 2967–2974. [CrossRef]
28. Uslu, I.; Comert, H.; Ipek, M.; Celebi, F.; Ozdemir, O.; Bindal, C. A comparison of borides formed on AISI 1040 and AISI P20 steels. *Mater. Des.* **2007**, *28*, 1819–1826. [CrossRef]
29. Gunes, I.; Kanat, S. Diffusion kinetics and characterization of borided AISI D6 steel. *Prot. Met. Phys. Chem. Surf.* **2015**, *51*, 842–846. [CrossRef]
30. Sen, S.; Sen, U.; Bindal, C. An approach to kinetic study of borided steels. *Surf. Coat. Technol.* **2005**, *191*, 274–285. [CrossRef]
31. Keddam, M.; Kulka, M. Boriding kinetics of AISI D2 steel by using two different approaches. *Met. Sci. Heat Treat.* **2020**, *61*, 756–763. [CrossRef]
32. Keddam, M.; Topuz, P. A kinetic approach for assessing boron diffusivities in iron boride layers formed on 34CrAlNi7 steel. *J. Chem. Technol. Metall.* **2022**, *57*, 824–833.
33. Keddam, M.; Topuz, P.; Aydin, Ö. Simulation of boronizing kinetics of AISI 316 steel with an integral diffusion model. *Mater. Test.* **2021**, *63*, 906–912. [CrossRef]
34. Keddam, M.; Hudáková, M.; Ptačinová, J.; Kusy, M.; Jurči, P. Modelling of the Boronizing Kinetics of Vanadis 6 Steel by the Integral Diffusion Model. *Prot. Met. Phys. Chem. Surf.* **2022**, *58*, 347–355. [CrossRef]
35. Yu, L.; Chen, X.; Khor, K.; Sundararajan, G. FeB/Fe2B phase transformation during SPS pack-boriding: Boride layer growth kinetics. *Acta Mater.* **2005**, *53*, 2361–2368. [CrossRef]
36. Abdellah, Z.N.; Chegroune, R.; Keddam, M.; Bouarour, B.; Haddour, L.; Elias, A. The Phase Stability in the Fe-B Binary System: Comparison between the Interstitial and Substitutional Models. *Defect Diffus. Forum* **2012**, *322*, 1–9. [CrossRef]
37. Press, W.H.; Flannery, B.P.; Teukolsky, S.A.; Vetterling, W. *Numerical Recipes in Pascal: The Art of Scientific Computing*; Cambridge University Press: New York, NY, USA, 1989; Volume 781.
38. Kunst, H.; Schaaber, O. Beobachtungen beim Oberflaechenborieren von Stahl. *Haerterei Tech. Mitt.* **1967**, *22*, 1–25.
39. Boumaali, B.; Nait, A.Z.; Keddam, M. Characterization of bilayer (FeB/Fe2B) on AISI H13 work tool steel. *Koroze Ochr. Mater.* **2021**, *65*, 40–48. [CrossRef]
40. Kulka, M. *Current Trends in Boriding Techniques*; Springer: Cham, Switzerland, 2019.
41. Kayali, Y.; Talaş,, Ş; Yalçin, M.C.; Kul, M.; Yazar, M.; Kir, H. Diffusion Kinetics of Boronized ASP®2012 Tool Steel Produced by Powder Metallurgy. *Prot. Met. Phys. Chem. Surf.* **2022**, *58*, 1036–1043. [CrossRef]
42. Keddam, M.; Jurči, P. Simulating the Growth of Dual-Phase Boride Layer on AISI M2 Steel by Two Kinetic Approaches. *Coatings* **2021**, *11*, 433. [CrossRef]
43. Kayalı, Y.; Kara, R. Investigation of Wear Behavior and Diffusion Kinetic Values of Boronized Hardox-450 Steel. *Prot. Met. Phys. Chem. Surf.* **2021**, *57*, 1025–1033. [CrossRef]
44. Türkmen, I.; Yalamaç, E.; Keddam, M. Investigation of tribological behaviour and diffusion model of Fe2B layer formed by the pack-boriding process on SAE 1020 steel. *Surf. Coat. Technol.* **2019**, *377*, 124888. [CrossRef]
45. Arslan, M.; Karimzadehkhoei, M.; Sireli, G.K.; Coskun, O.K.; Sert, M.; Timur, S. Investigating Growth of Iron Borides with the Formation of Monolithic Fe2B Layer on AISI 304 Stainless Steel via Cathodic Reduction and Thermal Diffusion-Based Boriding. *J. Mater. Eng. Perform.* **2022**, *31*, 3274–3286. [CrossRef]

46. Keddam, M.; Chegroune, R.; Kulka, M.; Makuch, N.; Panfil, D.; Siwak, P.; Taktak, S. Characterization, Tribological and Me-chanical Properties of Plasma Paste Borided AISI 316 Steel. *Trans. Indian Inst. Met.* **2017**, *71*, 79–90. [CrossRef]
47. Campos-Silva, I.; Hernández-Ramirez, E.; Contreras-Hernández, A.; Rosales-Lopez, J.; Valdez-Zayas, E.; Mejía-Caballero, I.; Martínez-Trinidad, J. Pulsed-DC powder-pack boriding: Growth kinetics of boride layers on an AISI 316 L stainless steel and Inconel 718 superalloy. *Surf. Coat. Technol.* **2021**, *421*, 127404. [CrossRef]

Disclaimer/Publisher's Note: The statements, opinions and data contained in all publications are solely those of the individual author(s) and contributor(s) and not of MDPI and/or the editor(s). MDPI and/or the editor(s) disclaim responsibility for any injury to people or property resulting from any ideas, methods, instructions or products referred to in the content.